Intelligent Equipment and Special Robots
Q. Zhang (Ed.)

doi:10.3233/ATDE240237

Kinematic Performance Optimization of Double Wishbone Suspension Based on ADAMS

Shihao SUN, Yan ZHU[1], Juan DU, Zhaozhuang JIANG
School of Mechanical and Automotive Engineering, Liaocheng University, Liaocheng 252000, China

Abstract. Use ADAMS software to optimize the suspension kinematic parameters to make a certain double wishbone suspension have superior kinematic performance. Firstly, establish a suspension simulation model in ADAMS/Car and make wheel jump simulations for the model. Upon completion of the simulation, ADAMS/PostProcessor delivers the change range of the 4 main kinematic parameters of double wishbone suspension: Toe Angle, Camber Angle, Kingpin Caster Angle, and Kingpin Inclination Angle. Secondly, choose the variable points coordinates. ADAMS/Car and ADAMS/Insight jointly optimized the coordinates. Thirdly, the two wheel jump simulations of the coordinate-optimized suspension are carried out again, and after the simulations, the optimization data of the 4 kinematic parameters are obtained. Finally, analyze the optimization data and evaluate the kinematic performance of the optimized double wishbone suspension. After the optimization, four suspension kinematic parameters change range are basically within the ideal range. This optimization has achieved the excellent results, and at the same time, it provides ideas and reference significance for the optimization of other types of suspensions.

Keywords. ADAMS, the double wishbone suspension, kinematic parameters, parameters optimization

1. Introduction

The suspension is the critical component of the vehicles. The important purpose of setting the suspension is to isolate the passengers from the vibration and to enhance the vehicle's driving grip [1]. Double wishbone suspension, which is suitable for passenger cars and racing cars, has high strength and impact resistance [2]. The main kinematic characteristic performance of suspension is the regular change of kinematic parameters such as wheel positioning in the process of wheel runout. This is a key reference standard for the performance of vehicle driving stability and ride comfort [3]. Therefore, the optimization of double wishbone suspension kinematic parameters has great significance.

Many scholars have done a lot of research on suspension optimization. Based on the principle of virtual work, Lv Jintian optimized the kinematic performance of suspension by analyzing the mechanical balance relationship [4]. Based on multi-body dynamics, Ding Jinquan et al proposed an active righting control algorithm to accelerate the speed

[1] Corresponding author: Yan ZHU, School of Mechanical and Automotive Engineering, Liaocheng University, e-mail: 444981419@qq.com

of wheel righting [5]. In reference [6], a new multi-objective archive-based Quantum Particle Optimizer improves suspension optimization. In reference [7], an improved chaos particle swarm optimization is proposed to optimize the suspension parameters.

Based on the physical model, ADAMS software can combine, analyze, and display the changes of the simulation physical model in a certain process and provides a variety of "virtual prototype" solutions [8], which can reduce the time and capital investment for product research. Therefore, in this paper, wheel jump tests based on ADAMS software are carried out on a double wishbone suspension model to improve the kinematic performance of the suspension.

2. Double Wishbone Suspension Wheel Jump Simulation

2.1 Double wishbone suspension model

2.1.1. Double wishbone suspension 3D model

Establish the double wishbone suspension 3D model in SOLIDWORKS. The 3D model is shown in Figure 1.

2.1.2. Establish the structure diagram of the model

Simplify the 3D model appropriately. Figure 2 shows the structural sketch of the double wishbone suspension. Point A is the front point of the upper control arm, point B is the rear point of the upper control arm, point C is the outer point of the upper control arm, point D is the front point of the lower control arm, point E is the rear point of the lower control arm, point F is the outer point of the lower control arm, point G is the wheel center point, point H is the outer point of steering tie rod, point I is the inner point of tie rod, point J is the top mount point, and point K is the strut lower point.

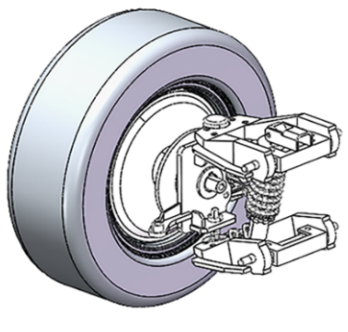

Figure 1. Double wishbone suspension 3D model

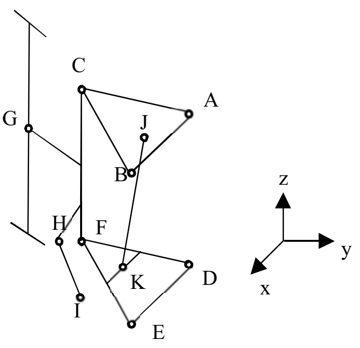

Figure 2. Suspension structure sketch diagram

2.1.3 Establish simulation model

Use SOLIDWORKS to measure the key hard point coordinates of the double wishbone suspension. The coordinates are shown in Table 1.

Table 1. Suspension hard point coordinates

Hard point	x. coordinate /mm	y. coordinate/mm	z. coordinate /mm
Lca_ front	-93.5	-354.2	222.5
Lca_ outer	0	-563	162
Lca_ rear	93.5	-354.2	222.5
Strut_ lower	1.3	-486.5	213.5
Tierod_ inner	200	-400	257
Tierod_ outer	175	-556.133	257.43
Top_ mount	2.6	-381.7	475
Uca_ front	-93.5	-314.7	442.5
Uca_ outer	0	-558.71	440
Uca_ rear	93.5	-314.7	442.5
Wheel_ center	0	-757	300

According to the hard point coordinates, create the simulation model in ADAMS/Car, as shown in Figure 3.

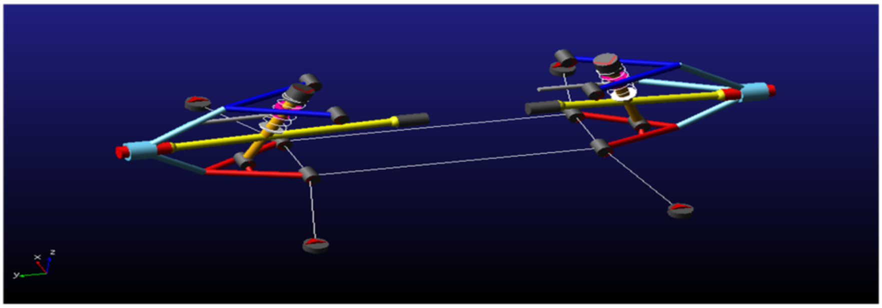

Figure 3. Double wishbone suspension simulation model

2.2 Simulation analysis of double wishbone suspension wheel jump test

2.2.1 Simulation test

We used ADAMS/Car to make parallel wheel jump and opposite wheel jump simulations for the suspension model. In the simulations, the upper runout and lower runout are set to ±50mm, and the simulation step is set to 100 steps.

2.2.2 Analysis of suspension kinematic parameters

Double wishbone suspension's kinematic performance mainly depends on four parameters, namely Toe Angle, Camber Angle, Kingpin Caster Angle and Kingpin Inclination Angle [9]. Toe Angle is the angle between the vehicle longitudinal axis and the direction which the vehicle's wheels are pointing when viewed from above. It can reduce the wear of the type and its ideal range is -0.5° ~ 0.5°. Camber Angle is the angle between the wheel plane and the vehicle plane when viewed from the front. It can reduce the wheel steering offset to improve the safety of vehicle movement and its ideal range is -2° ~ 2°. Kingpin Caster Angle is the angle between the kingpin axis and the road plane vertical of the vehicle's longitudinal plane. It can keep the stability of the vehicle and its ideal range is 0° ~ 6°. Kingpin Inclination Angle is the angle between the kingpin axis and the road plane vertical of the vehicle's lateral plane. It can make wheels positivea and its ideal range is 5° ~ 10° [10~14].

2.2.3 Determine the targeted parameters

Use ADAMS/PostProcessor to obtain the simulation results of double wishbone suspension. The kinematic parameters data is shown in Table 2. According to Table. 2, in two simulations, the Toe Angle, Camber Angle, and Kingpin Inclination Angle are out of their ideal range. Therefore, set them as the targeted parameters of this optimization.

Table 2. Parameter range before optimization

Parameter /°	parallel wheel jump		opposite wheel jump	
	range	variation	range	variation
Toe Angle	-3.20～1.60	4.80	-3.30～1.70	5.10
Camber Angle	-2.50～2.10	4.60	-2.50～2.10	4.60
Kingpin Caster Angle	0.10～0.40	0.30	0.10～0.40	0.30
Kingpin Inclination Angle	-1.30～3.42	4.72	-1.27～3.40	4.67

3. Optimization of Double Wishbone Suspension

3.1. Select optimization point coordinates

The hard point coordinates are also important influencing factors of suspension kinematic parameters [15]. Therefore, the optimization of suspension in this paper starts from the hard point coordinates optimization.

Nine points that significantly influence suspension kinematic parameters are selected as variable points: Tierod_ inner. z, Tierod_ outer. z, Uca_ front. z, Lca_ rear. z, Uca_ outer. z, Uca_ rear. z, Lca_ front. z, Uca_ rear. x and Uca_ front. x.

3.2. Model fitting

ADAMS/Insight can evaluate whether the simulation model is reliable using the four values of R2, R2adj, P, and R/V. The values of R2 and R2adj are between 0 and 1, and the larger the better; the smaller the value of P, the more valuable terms it has, the value of R/V should be greater than 4, and the larger the better [16].

The simulation model is fitted in ADAMS/Insight, and its reliable values are shown in Table 3.

Table 3. Reliable values of the simulation model

Parameter	Test	R2	R2adj	P	R/V
Toe Angle	parallel wheel jump	0.999	0.999	0	853
	opposite wheel jump	0.999	0.999	0	776
Camber Angle	parallel wheel jump	0.999	0.999	0	987
	opposite wheel jump	0.999	0.999	0	1090
Kingpin Caster Angle	parallel wheel jump	0.999	0.999	0	869
	opposite wheel jump	0.999	0.999	0	813
Kingpin Inclination Angle	parallel wheel jump	0.999	0.999	0	1000
	opposite wheel jump	0.999	0.999	0	1000

From Table 3, the values of R2 and R2adj are both 0.999, the value of P is 0, and the value of R/V is much larger than 4. Therefore, the simulation model is reliable.

3.3. Optimize fixed point coordinates

Use ADAMS/Insight to analyze the sensitivity of 9 fixed point coordinates. Figures. 4 to 11 show the influenceable degree of 9 fixed point coordinates on the Toe Angle, Camber Angle, Kingpin Caster Angle, and Kingpin Inclination Angle.

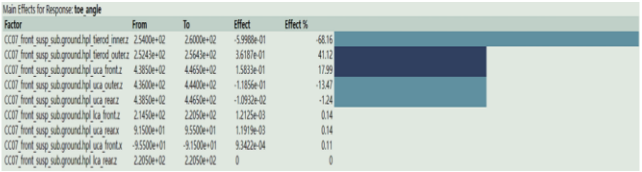
Main Effects for Response: **toe_angle**

Factor	From	To	Effect	Effect %
CC07_front_susp_sub.ground.hpl_tierod_inner.z	2.5400e+02	2.6000e+02	-5.9988e-01	-68.16
CC07_front_susp_sub.ground.hpl_tierod_outer.z	2.5243e+02	2.5643e+02	3.6187e-01	41.12
CC07_front_susp_sub.ground.hpl_uca_front.z	4.3850e+02	4.4650e+02	1.5833e-01	17.99
CC07_front_susp_sub.ground.hpl_uca_outer.z	4.3600e+02	4.4400e+02	-1.1856e-01	-13.47
CC07_front_susp_sub.ground.hpl_uca_rear.z	4.3850e+02	4.4650e+02	-1.0932e-02	-1.24
CC07_front_susp_sub.ground.hpl_lca_front.z	2.1450e+02	2.2050e+02	1.2125e-03	0.14
CC07_front_susp_sub.ground.hpl_uca_rear.x	9.1500e+01	9.5500e+01	1.1919e-03	0.14
CC07_front_susp_sub.ground.hpl_uca_front.x	-9.5500e+01	-9.1500e+01	9.3422e-04	0.11
CC07_front_susp_sub.ground.hpl_lca_rear.z	2.2050e+02	2.2050e+02	0	0

Figure 4. The Toe Angle of the parallel wheel jump

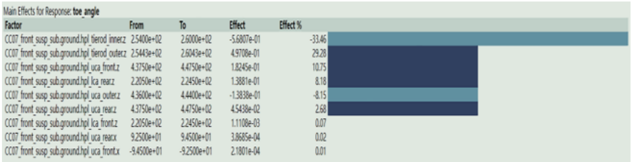
Main Effects for Response: **toe_angle**

Factor	From	To	Effect	Effect %
CC07_front_susp_sub.ground.hpl_tierod_inner.z	2.5400e+02	2.6000e+02	-5.6807e-01	-33.46
CC07_front_susp_sub.ground.hpl_tierod_outer.z	2.5443e+02	2.6043e+02	4.9708e-01	29.28
CC07_front_susp_sub.ground.hpl_uca_front.z	4.3750e+02	4.4750e+02	1.8245e-01	10.75
CC07_front_susp_sub.ground.hpl_lca_rear.z	2.2050e+02	2.2450e+02	1.3881e-01	8.18
CC07_front_susp_sub.ground.hpl_uca_outer.z	4.3600e+02	4.4400e+02	-1.3838e-01	-8.15
CC07_front_susp_sub.ground.hpl_uca_rear.z	4.3750e+02	4.4750e+02	4.5438e-02	2.68
CC07_front_susp_sub.ground.hpl_lca_front.z	2.2050e+02	2.2450e+02	1.1108e-03	0.07
CC07_front_susp_sub.ground.hpl_uca_rear.x	9.2500e+01	9.4500e+01	3.8685e-04	0.02
CC07_front_susp_sub.ground.hpl_uca_front.x	-9.4500e+01	-9.2500e+01	2.1801e-04	0.01

Figure 5. The Toe Angle of the opposite wheel jump

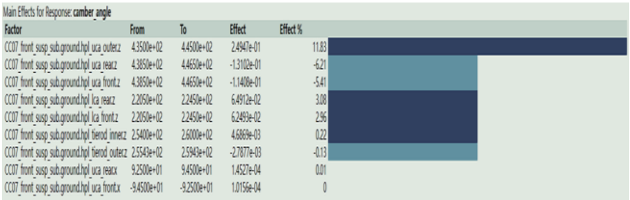
Main Effects for Response: **camber_angle**

Factor	From	To	Effect	Effect %
CC07_front_susp_sub.ground.hpl_uca_outer.z	4.3500e+02	4.4500e+02	2.4947e-01	11.83
CC07_front_susp_sub.ground.hpl_uca_rear.z	4.3850e+02	4.4650e+02	-1.3102e-01	-6.21
CC07_front_susp_sub.ground.hpl_uca_front.z	4.3850e+02	4.4650e+02	-1.1408e-01	-5.41
CC07_front_susp_sub.ground.hpl_lca_rear.z	2.2050e+02	2.2450e+02	6.4912e-02	3.08
CC07_front_susp_sub.ground.hpl_lca_front.z	2.2050e+02	2.2450e+02	6.2493e-02	2.96
CC07_front_susp_sub.ground.hpl_tierod_inner.z	2.5400e+02	2.6000e+02	4.6869e-03	0.22
CC07_front_susp_sub.ground.hpl_tierod_outer.z	2.5543e+02	2.5943e+02	-2.7877e-03	-0.13
CC07_front_susp_sub.ground.hpl_uca_rear.x	9.2500e+01	9.4500e+01	1.4527e-04	0.01
CC07_front_susp_sub.ground.hpl_uca_front.x	-9.4500e+01	-9.2500e+01	1.0156e-04	0

Figure 6. The Camber Angle of the parallel wheel jump

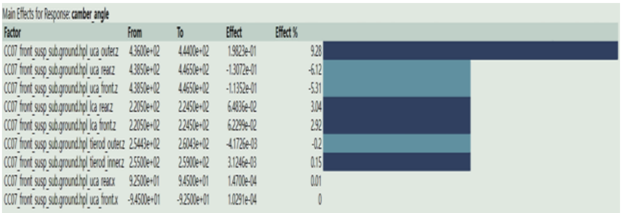
Main Effects for Response: **camber_angle**

Factor	From	To	Effect	Effect %
CC07_front_susp_sub.ground.hpl_uca_outer.z	4.3600e+02	4.4400e+02	1.9823e-01	9.28
CC07_front_susp_sub.ground.hpl_uca_rear.z	4.3850e+02	4.4650e+02	-1.3072e-01	-6.12
CC07_front_susp_sub.ground.hpl_uca_front.z	4.3850e+02	4.4650e+02	-1.1352e-01	-5.31
CC07_front_susp_sub.ground.hpl_lca_rear.z	2.2050e+02	2.2450e+02	6.4836e-02	3.04
CC07_front_susp_sub.ground.hpl_lca_front.z	2.2050e+02	2.2450e+02	6.2299e-02	2.92
CC07_front_susp_sub.ground.hpl_tierod_outer.z	2.5443e+02	2.6043e+02	-4.1726e-03	-0.2
CC07_front_susp_sub.ground.hpl_tierod_inner.z	2.5500e+02	2.5900e+02	3.1246e-03	0.15
CC07_front_susp_sub.ground.hpl_uca_rear.x	9.2500e+01	9.4500e+01	1.4700e-04	0.01
CC07_front_susp_sub.ground.hpl_uca_front.x	-9.4500e+01	-9.2500e+01	1.0291e-04	0

Figure 7. The Camber Angle of the opposite wheel jump


Main Effects for Response: **caster_angle**

Factor	From	To	Effect	Effect %
CC07_front_susp_sub.ground.hpl_uca_rear.z	4.3850e+02	4.4650e+02	1.5799e-01	30.38
CC07_front_susp_sub.ground.hpl_uca_front.z	4.3850e+02	4.4650e+02	-1.5120e-01	-29.08
CC07_front_susp_sub.ground.hpl_lca_front.z	2.2050e+02	2.2450e+02	6.8702e-02	13.21
CC07_front_susp_sub.ground.hpl_lca_rear.z	2.2050e+02	2.2450e+02	-5.8315e-02	-11.21
CC07_front_susp_sub.ground.hpl_uca_outer.z	4.3600e+02	4.4400e+02	-2.2682e-02	-4.36
CC07_front_susp_sub.ground.hpl_uca_rear.x	9.2500e+01	9.4500e+01	-4.8860e-03	-0.94
CC07_front_susp_sub.ground.hpl_tierod_outer.z	2.5443e+02	2.6043e+02	2.5871e-03	0.5
CC07_front_susp_sub.ground.hpl_tierod_inner.z	2.5500e+02	2.5900e+02	-1.5211e-03	-0.29
CC07_front_susp_sub.ground.hpl_uca_front.x	-9.4500e+01	-9.2500e+01	-1.2149e-03	-0.23

Figure 8. The Caster Angle of the parallel wheel jump

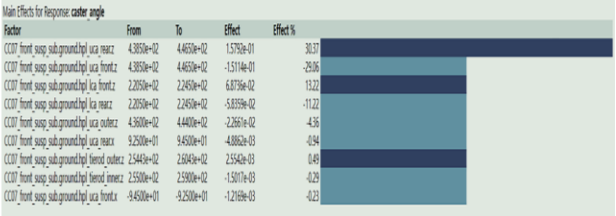

Main Effects for Response: **caster_angle**

Factor	From	To	Effect	Effect %
CC07_front_susp_sub.ground.hpl_uca_rear.z	4.3850e+02	4.4650e+02	1.5792e-01	30.37
CC07_front_susp_sub.ground.hpl_uca_front.z	4.3850e+02	4.4650e+02	-1.5114e-01	-29.06
CC07_front_susp_sub.ground.hpl_lca_front.z	2.2050e+02	2.2450e+02	6.8736e-02	13.22
CC07_front_susp_sub.ground.hpl_lca_rear.z	2.2050e+02	2.2450e+02	-5.8359e-02	-11.22
CC07_front_susp_sub.ground.hpl_uca_outer.z	4.3600e+02	4.4400e+02	-2.2661e-02	-4.36
CC07_front_susp_sub.ground.hpl_uca_rear.x	9.2500e+01	9.4500e+01	-4.8862e-03	-0.94
CC07_front_susp_sub.ground.hpl_tierod_outer.z	2.5443e+02	2.6043e+02	2.5542e-03	0.49
CC07_front_susp_sub.ground.hpl_tierod_inner.z	2.5500e+02	2.5900e+02	-1.5017e-03	-0.29
CC07_front_susp_sub.ground.hpl_uca_front.x	-9.4500e+01	-9.2500e+01	-1.2169e-03	-0.23

Figure 9. The Caster Angle of the opposite wheel jump

Main Effects for Response: **inclination_angle**

Factor	From	To	Effect	Effect %
CC07_front_susp_sub.ground.hpl_uca_outer.z	4.3560e+02	4.4440e+02	2.1952e-01	10.41
CC07_front_susp_sub.ground.hpl_uca_rear.z	4.3808e+02	4.4693e+02	-1.4487e-01	-6.87
CC07_front_susp_sub.ground.hpl_uca_front.z	4.3808e+02	4.4693e+02	-1.2616e-01	-5.98
CC07_front_susp_sub.ground.hpl_lca_rear.z	2.2028e+02	2.2473e+02	7.2190e-02	3.42
CC07_front_susp_sub.ground.hpl_lca_front.z	2.2028e+02	2.2473e+02	6.9508e-02	3.3
CC07_front_susp_sub.ground.hpl_tierod_inner.z	2.5443e+02	2.5957e+02	4.0236e-03	0.19
CC07_front_susp_sub.ground.hpl_tierod_outer.z	2.5486e+02	2.6000e+02	-3.5975e-03	-0.17
CC07_front_susp_sub.ground.hpl_uca_rear.x	9.2565e+01	9.4435e+01	1.3887e-04	0.01
CC07_front_susp_sub.ground.hpl_uca_front.x	-9.4435e+01	-9.2565e+01	9.3061e-05	0

Figure 10. The Inclination Angle of the parallel wheel jump

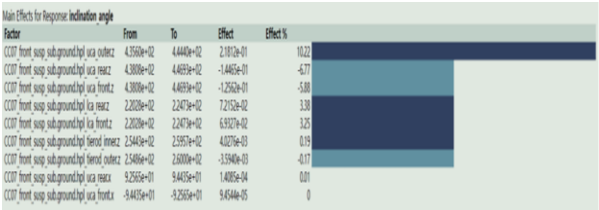

Main Effects for Response: **inclination_angle**

Factor	From	To	Effect	Effect %
CC07_front_susp_sub.ground.hpl_uca_outer.z	4.3560e+02	4.4440e+02	2.1812e-01	10.22
CC07_front_susp_sub.ground.hpl_uca_rear.z	4.3808e+02	4.4693e+02	-1.4465e-01	-6.77
CC07_front_susp_sub.ground.hpl_uca_front.z	4.3808e+02	4.4693e+02	-1.2562e-01	-5.88
CC07_front_susp_sub.ground.hpl_lca_rear.z	2.2028e+02	2.2473e+02	7.2152e-02	3.38
CC07_front_susp_sub.ground.hpl_lca_front.z	2.2028e+02	2.2473e+02	6.9327e-02	3.25
CC07_front_susp_sub.ground.hpl_tierod_inner.z	2.5443e+02	2.5957e+02	4.0276e-03	0.19
CC07_front_susp_sub.ground.hpl_tierod_outer.z	2.5486e+02	2.6000e+02	-3.5940e-03	-0.17
CC07_front_susp_sub.ground.hpl_uca_rear.x	9.2565e+01	9.4435e+01	1.4085e-04	0.01
CC07_front_susp_sub.ground.hpl_uca_front.x	-9.4435e+01	-9.2565e+01	9.4544e-05	0

Figure 11. The Inclination Angle of the opposite wheel jump

From Figures. 4 to 11, we can see that for Toe Angle, the Tierod_ inner. z, Tierod_ outer. z and Uca_ front. z are 3 most influenceable points. Tierod_ inner. z has 50.81% average degree impact, Tierod_ outer. z has 35.2% average degree impact and Uca_ front. z has 14.37% average degree impact; For Camber Angle, the Uca_ outer. z, Uca_ rear. z and Uca_ front. z are 3 most influenceable points. Uca_ outer. z has 10.54% average degree impact, Uca_ rear. z has 6.165% average degree impact and Uca_ front. z has 5.36% average degree impact; For Caster Angle, the Uca_ rear. z, Uca_ front. z and Lca_ front. z are 3 most influenceable points. Uca_ rear. z has 30.375% average degree impact, Uca_ front. z has 29.07% average degree impact and Lca_ front. z has 13.215% average degree impact; For Inclination Angle, the Uca_ outer. z, Uca_ rear. z and Uca_ front. z are 3 most influenceable points. Uca_ outer. z has 10.315% average degree impact, Uca_ rear. z has 6.82% average degree impact and Uca_ front. z has 5.93% average degree impact.

Jointly use ADAMS/Car and ADAMS/Insight to make multi-parameter optimization to optimize the 9 fixed point coordinates. The optimization results are shown in Table 4.

Table 4. Variables coordinates before and after optimization

Coordinate	Before optimization/mm	After optimization/mm
Tierod_inner. z	257	251.43
Tierod_outer. z	257.43	245.43

Uca_front. z	442.5	443.5
Lca_rear. z	222.5	203.5
Uca_outer. z	440	444
Uca_rear. z	442.5	443.5
Lca_front. z	222.5	203.5
Uca_rear.x	93.5	92.5
Uca_front.x	-93.5	-92.5

4. Optimization Results

Modifying the hard point coordinates in ADAMS/Car and performing the wheel jump test on the simulation model again. After the test, organize the data of before optimization and after optimization into Table 5.

Table 5. Kinematic parameters comparison before and after optimization

Parameter/°			Parallel wheel jump	Opposite wheel jump
Toe Angle	range	Before	-3.20 ~ 1.60	-3.30 ~ 1.70
		After	-0.47 ~ 0.45	-0.47 ~ 0.52
	variation	Before	4.80	5.10
		After	0.92	0.99
Camber Angle	range	Before	-2.50 ~ 2.10	-2.50 ~ 2.10
		After	-1.08 ~ 0.7	-1.08 ~ 0.7
	variation	Before	4.60	4.60
		After	1.78	1.78
Kingpin Caster Angle	range	Before	0.10 ~ 0.40	0.10 ~ 0.40
		After	0.13 ~ 0.29	0.14 ~ 0.30
	variation	Before	0.30	0.30
		After	0.16	0.16
Kingpin Inclination Angle	range	Before	-1.30 ~ 3.42	-1.27 ~ 3.40
		After	4.60 ~ 6.50	4.60 ~ 6.50
	variation	Before	4.72	4.67
		After	1.90	1.90

From Table 5, after optimization, we can observe: Toe Angle in the two tests is basically within ideal range. In parallel jump test, Toe Angel becomes -0.47°~0.45°, and variation amount is reduced by 80.8%. In opposite jump test, Toe Angle becomes -0.47°~0.52°, and variation amount is reduced by 80.6%. Compared with before optimization, the change of Toe Angle is significantly reduced; Camber Angle in both tests is within ideal range. In both tests, Camber Angle becomes -1.08°~0.7°, within ideal range. At the same time, variation amount is reduced by 61.3%. After optimization, Camber Angle becomes more ideal; Kingpin Caster Angle in two tests is within ideal range. Kingpin Caster Angle is reduced from 0.30°to 0.16°, through optimization, making the change of Kingpin Caster Angle more stable; Kingpin Inclination Angle in the two tests is basically within ideal range. In parallel wheel jump test, Kingpin Inclination Angle becomes 4.60°~6.50°, and variation is decreased by 59.7%. In opposite wheel jump test, variation range becomes 4.60°~6.50°, and variation amount is decreased by 59.3%. After optimization, although Kingpin Inclination Angle is basically within ideal range, it is in the edge position of ideal range. This is because ADAMS/Insight needs to consider benefits of each parameter when optimizing double wishbone suspension.

5. Conclusions

After optimization: In parallel jump simulation, Toe Angle becomes -0.47 ° ~ 0.45 °, Camber Angle becomes -1.08 ° ~ 0.7 °, Kingpin Caster Angle becomes -0.13 ° ~ 0.29 °, and Kingpin Inclination Angle becomes 4.60 ° ~ 6.50 °. In opposite jump simulation, Toe Angle becomes -0.47 ° ~ 0.52 °, Camber Angle becomes -1.08 ° ~ 0.7 °, Kingpin Caster Angle becomes -0.14 ° ~ 0.30 °, and Kingpin Inclination Angle becomes 4.60 ° ~ 6.50 °. The kinematic performance of the double wishbone suspension has been significantly improved, effectively improving the stability of the vehicle.

Acknowledgement

This work was supported by the Fundamental Research Funds for the Central Universities (300102221503, K21LC0301); Scientific Research Fund of Liaocheng University;(311102133,311101910); Innovation and Entrepreneurship Training Program for College Students of Liaocheng University (CXCY2023146).

References

[1] Niu Zhihua; Jin Sun; Wang Rongrong; Zhang Yansong. (2022). Geometry optimization of a planar double wishbone suspension based on whole-range nonlinear dynamic model. Proceedings of the Institution of Mechanical Engineers, Part D: Journal of AutomobileEngineering 236(4), 569-581, doi:10.1177/09544070211026205.

[2] LI Fei, WU Huawei, JIANG Jie. (2018). Design of Double Wishbone Suspension System for FSAE Racing Car. Journal of Chongqing University of Technology (Natural Science) 32(05), 77-81, doi:10.3969/j.issn.1674-8425(z).2018.05.012.

[3] HONG Chao, JIANG Weng, YU Yichang. (2017). The Spatial Geometric Analysis and Simulation Analysis of the Five-link Front Suspension System. Shanghai Auto 12, 8-11, doi:10.3969/j.issn.1007-4554.2017.12.02.

[4] LV Jintian. (2022). A fast Suspension Kinematics Analysis Method based on Virtual Work Principle. Auto Time 01, 142-144, doi:10.3969/j.issn.1672-9668.2022.01.066.

[5] DING Jinquan, XV Nan, GUO Konghui. (2016) Active return control based on imaginary king-pin kinematics calculation. Journal of Jilin University (Engineering and Technology Edition) 47, 21-27, doi:10.13229/j.cnki.jdxbgxb201701004.

[6] Ewerton Grotti, Douglas Makoto, Mizushima, Artur Dieguez Backes, Marcos Daniel de Freitas Awruch, Herbert Martins Gomes. (2020). A novel multi-objective quantum particle swarm algorithm for suspension optimization. Computational and Applied Mathematics 39(4),523-532, doi: 10.1007/s40314-020-1131-y.

[7] ZHANG Jun, LI Xin, LIU Duyou. (2020). Mine car suspension parameter optimisation based on improved particle swarm optimisation and approximation model. International Journal of Vehicle Design 80(1),23-40.

[8] Yang Baojian; Deng Yongning, Yue Xia, Teo Kenneth Tze Kin. (2021) 3D solid robot animation design based on ADAMS. International Journal of System Assurance Engineering and Management 14(2), 1-13, doi: 10.1007/S13198-021-01280-Y.

[9] LI Penglei, ZHOU Changcheng, LI Song, SUN (2022). Jiazheng. Kinematics Analysis and Optimization of Double Wishbone Suspension Guide Mechanism. Automobile Applied Technology 47(05), 54-57, doi:10.16638/j.cnki.1671-7988.2022.005.013.

[10] Hwangjae L, Ben S C. (2023). Online Detection of Toe Angle Misalignment Based on Lateral Tire Force and Tire Aligning Moment. International Journal of Automotive Technology 24(3), 623-632,doi:10.1007/S12239-023-0052-3.

[11] Balabina T A, Karelina M Yu, Mamaev A N. (2021). Kinematic and power characteristics of the elastic wheel while rolling with camber and convergence. IOP Conference Series: Materials Science and Engineering 1159(1), doi:10.1088/1757-899X/1159/1/012069.

[12] CHEN Qiping, KANG Sheng, et al. (2020). Research on modeling and optimization simulation analysis of micro electric vehicle suspension. Journal of Vibroengineering 22(4), 923—932, doi: 10.21595/jve.2020.20522.
[13] KANG Xuezhong. (2023). Simulation and Optimization of Double-arm front suspension Based on ADAMS/Insight. Automobile Applied Technology 48(02), 62-66, doi:10.16638/j.cnki.1671-7988.2023.02.011.
[14] ZHENG Xijiang, JI Shaobo, LI Shu-ting, ZHANG Hong-wei. (2019). Effects Analysis of Front Axle's Alignment Parameters Change on Handling Stability. Machinery Design & Manufacture 07,263-267, doi: 10.19356/j.cnki.1001-3997.2019.07.064.
[15] ZHANG Xiang, YE Yvxiang. (2021). Optimization Analysis of Hard Point Coordinates and Bushing Stiffness of Multi-link Suspension. Agricultural Equipment &Vehicle Engineering 59(05), 63-67, doi: 10.3969/j.issn.1673-3142.2021.05.015.
[16] ZHAO Bofan, DONG Zhiming. (2022). Research on Optimization of Double Wishbone Front Suspension of Mining Track Based on ADAMS. Coal Mine Machinery 43(09), 136-138, doi:10.13436/j.mkjx.202209040.